Direct Spatial Imaging of Vortices in a Superconducting Wire Network

H. D. Hallen,* R. Seshadri, A. M. Chang, R. E. Miller, L. N. Pfeiffer, K. W. West, C. A. Murray, and H. F. Hess

AT&T Bell Laboratories, Murray Hill, New Jersey 07974-0636

(Received 14 June 1993)

We report direct observations of vortices in a square superconducting wire grid imaged using scanning Hall probe microscopy. Real space images of vortex configurations are obtained as a function of the flux per unit cell f by measuring the local magnetic field just above the sample. At $f=1/2$ we observe domains of the checkerboard ground state. As f is reduced from 1/2 to 1/3 vacancies first penetrate the grain boundaries and then the checkerboard domains. Near $f=1/3$ we observe domains of the 1/3 staircase ground state. Heating the sample close to T_c produces correlated vortex hopping.

PACS numbers: 74.60.Ge, 61.16.Ch, 74.25.Ha, 74.80.−g

Two-dimensional superconducting wire networks have been studied extensively in the past decade [1–4]. The ability to vary experimental parameters, such as the size and symmetry of the network and the flux per unit cell or frustration f, makes these networks attractive and convenient for detailed investigation. The effects of f on the superconducting transition have been studied theoretically with a frustrated xy model of the phase of the superconducting order parameter, and detailed predictions for ground state vortex configurations at rational f fractions have been made [1–3]. However, past experimental studies of these networks [4] were limited to macroscopic transport measurements and average magnetic behavior because microscopic vortex configurations were experimentally inaccessible.

In this Letter we present direct observations of the vortex configurations in a superconducting wire network as a function of the frustration f using high-resolution scanning Hall probe microscopy. In a perpendicular magnetic field B a fraction $f(B)$ of the grid holes in the square superconducting wire grid are penetrated by a flux quantum. We observe these vortices in individual grid holes, and image their spatial distribution in a field of view containing ~400 squares. At fillings $f=1/2$ and $f=1/3$ the domains observed are consistent with predicted ground state configurations [1–3]. For higher order fractions we do not observe large ordered regions possibly due to the difficulty of equilibrium. We also find that heating the sample close to T_c produces correlated vortex hopping.

The sample was a 100×200 element square grid of 0.25 μm wide niobium wires with a 0.95 μm periodicity. It was fabricated by patterning a 1000 Å thick Nb film on a sapphire substrate using electron beam lithography and reactive ion etching. The Nb has a superconducting transition temperature $T_c=8.8$ K at $B=0$ G, a room temperature resistivity of 1.5 ± 0.5 Ω/square, and a resistivity ratio at 300 to 10 K of ~2. To test sample quality and calibrate the filling from the applied perpendicular magnetic field B, we performed *in situ* four-point transport measurements. The measured variation of T_c as a function of B is similar to previous reports [5]: T_c is periodic in the field $B=22.6$ G and corresponds to $f=1$ (and defines the 0.95 μm period) with substructures at $f=1/2$ and $f=1/3$.

Experiments were done by cooling the sample slowly (~1 mK/sec) in the applied field B of a persistent superconducting magnet to below T_c. We then used a scanning Hall probe microscope [6] to detect the local magnetic field above the sample. The probe, a GaAs heterostructure patterned into a Hall bar by electron beam lithography (0.3 μm square junction), was positioned 0.22 μm above the sample surface and then raster scanned to record the local-field-induced Hall voltage. The images were acquired well below T_c at a temperature $T=5$ K, where the vortex configurations are observed to be identical after repeated imaging and where the flux is tightly confined. The probe is relatively noninvasive with a maximum perturbative field imposed on the sample of 5×10^{-4} G.

Figure 1 shows real space images of vortex configurations obtained at different values of filling. Shown in the top row of Fig. 1 are the Hall voltage data with gray scale values proportional to measured local magnetic fields. The second row in Fig. 1 shows corresponding occupancy maps: Each square in a grid is colored white if occupied by a vortex and gray if empty. The value of f indicated was determined by the applied field B and confirmed by measured vortex densities. To create the occupancy maps from the raw data, we identified the position of each vortex by its magnetic field profile within the grid. The size and orientation of the grid relative to the scan direction were confirmed by using the Hall bar as a scanning tunneling microscope. Figure 1(a) taken at $B=0$ G ($f=0$) contains three isolated vortices: two vortices and one antivortex. Since the sensitivity of the Hall probe and its position above the sample are well characterized, a fit to the measured field profile of an isolated vortex (amplitude ~5 G) indicates that only a fraction (~40%) of a flux quantum is confined to the grid hole containing the vortex center. The remaining flux penetrates across the 0.25 μm wires into neighboring holes with an effective film penetration depth λ_{eff} of ~0.2 μm. This is consistent with an independent estimate of λ_{eff} based on the sample resistance [7]. The fitted field

0031-9007/93/71(18)/3007(4)$06.00

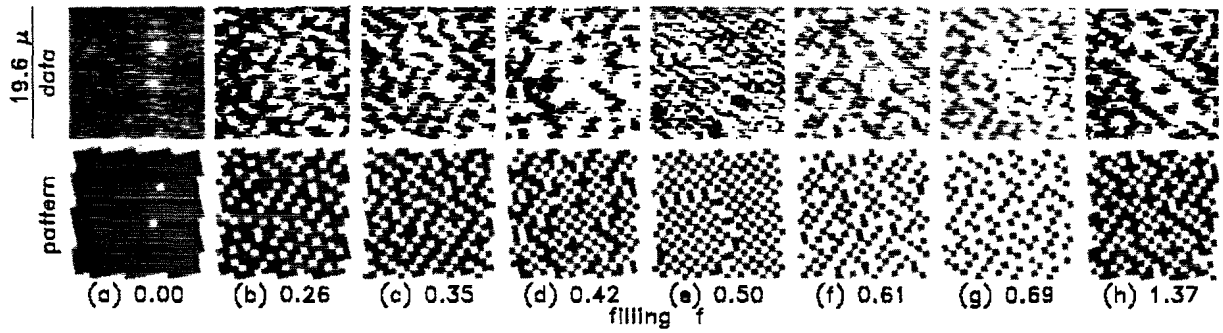

FIG. 1. Top row shows images (size 19.6 μm) of vortex configurations in a superconducting Nb wire grid of 0.95 μm×0.95 μm square holes obtained using scanning Hall probe microscopy at the filling fractions f indicated. The gray scale values correspond to the local magnetic field measured just above the sample. The second row shows the occupancy maps of the images: A square in a grid is colored white if it contains a vortex and gray if it is empty.

profile of such isolated vortices was used to determine vortex occupancy in a grid: Starting with the most prominent vortex, we successively subtracted the fitted field profile from the raw data at the site of each new vortex located, until the positions of all vortices in a given image were uniquely identified.

The most striking vortex configurations are observed near $f=1/2$ and $f=1/3$ [see Figs. 1(c) and 1(e)]. The largest domains are observed near $f=1/2$, where alternate grid holes are occupied to form a checkerboard pattern. In Fig. 1(e) at $f=0.50$ the two degenerate phases of the 1/2 checkerboard ground state, described theoretically by Teitel and Jayaprakash [2] (JT), are separated by a grain boundary. In Fig. 1(c) at $f=0.35$ (near 1/3) we observe the predicted JT 1/3 staircase patterns in which diagonal rows of vortices are spaced by two empty rows. Configurations similar to the 1/3 state are observed in Figs. 1(g) and 1(h) at $f=0.69$ (near 2/3, with occupied and empty sites reversed) and at $f=1.37$ (near 4/3). In the same manner, the configuration in Fig. 1(d) at $f=0.42$ (near 2/5) resembles that in Fig. 1(f) at $f=0.61$ (near 3/5, reversed). In Fig. 1(b) at $f=0.26$ (near 1/4) the vortex density is low and the configuration is disordered.

Figure 2 shows the evolution of vortex configurations as f varies from 1/3 to 1/2. We highlight the coordination, the 1/2 state domains, and the 1/3 state domains of this sequence in the different rows of Fig. 2. The row labeled "pattern" shows the occupation maps at the values of f indicated. In the top row each vortex is assigned a color corresponding to the occupation n of the eight adjacent sites. The row labeled "1/2" shows data masked by the predicted JT 1/2 checkerboard ground state [2], which has two possible phases colored yellow and blue. The rows labeled "1/3R" and "1/3L" show data masked by the two degenerate JT 1/3 staircase ground states [2], each of which has three possible phases colored yellow, blue, and pink.

At $f=0.50$ we see large checkerboard grains with only a few interstitials, vacancies, and grain boundaries [see Fig. 2(h) row 1/2, also Fig. 1(e)]. As f decreases below 0.5, in Figs. 2(g) and 2(f), the checkerboard grains become smaller in size and the added vacancies accumulate predominantly along grain boundaries. A further decrease [Fig. 2(e)] results in some vacancies penetrating the checkerboard grains. At yet lower f the checkerboard grains become even smaller and more porous, until in Fig. 2(a) at $f=0.34$ we observe alternating narrow diagonal stripes of the two checkerboard phases.

The 1/3 staircase grains near $f=1/3$ [see Fig. 2(a) rows 1/3R and 1/3L] are not as large as the checkerboard grains near $f=1/2$, perhaps because the 1/3 staircase state has six competing degenerate patterns instead of two in the checkerboard state, the six patterns have a larger nucleation size (the unit cell is 3×3 instead of 2×2 in the checkerboard), and domain walls between the six patterns are inexpensive compared to energetically expensive checkerboard grain boundaries. The 1/3L and 1/3R rows in Fig. 2 indicate that as f deviates from 0.33 the 1/3 staircase grains become small rapidly.

To quantify domain areas we measured the fraction of each image fit by the JT 1/2 checkerboard and 1/3 staircase states. The area coverage, measured by occupied sites, in units of the image size is plotted vs f in Fig. 3. Open symbols represent the expected coverage of the perfect 1/2 checkerboard and 3/7, 2/5, and 1/3 staircase JT ground states by 1/2 and 1/3 domains. As shown the 1/2 checkerboard state fills the entire image near $f=0.50$ and covers over 80 unit cells. As f decreases the image area covered by the checkerboard state (now reduced to diagonal lines) gradually decreases to the expected value of 2/3 near $f=0.33$. The 1/3 staircase fits the image well near $f=0.33$ (the largest domain covering about 20 unit cells) and the coverage drops to zero at $f=0.50$. Grains of the higher order 2/5 staircase state are always small (in the number of unit cells) perhaps because there are now ten competing degenerate patterns with a large nucleation size (unit cell is 5×5).

The single domain JT 1/2 checkerboard, JT 1/3, 2/5, and 3/7 staircase, and the Kolahchi and Straley (KS) [3] 3/7 vacancy-array theoretical ground states shown at the left [2,3] of Fig. 4. We characterize the local order of the

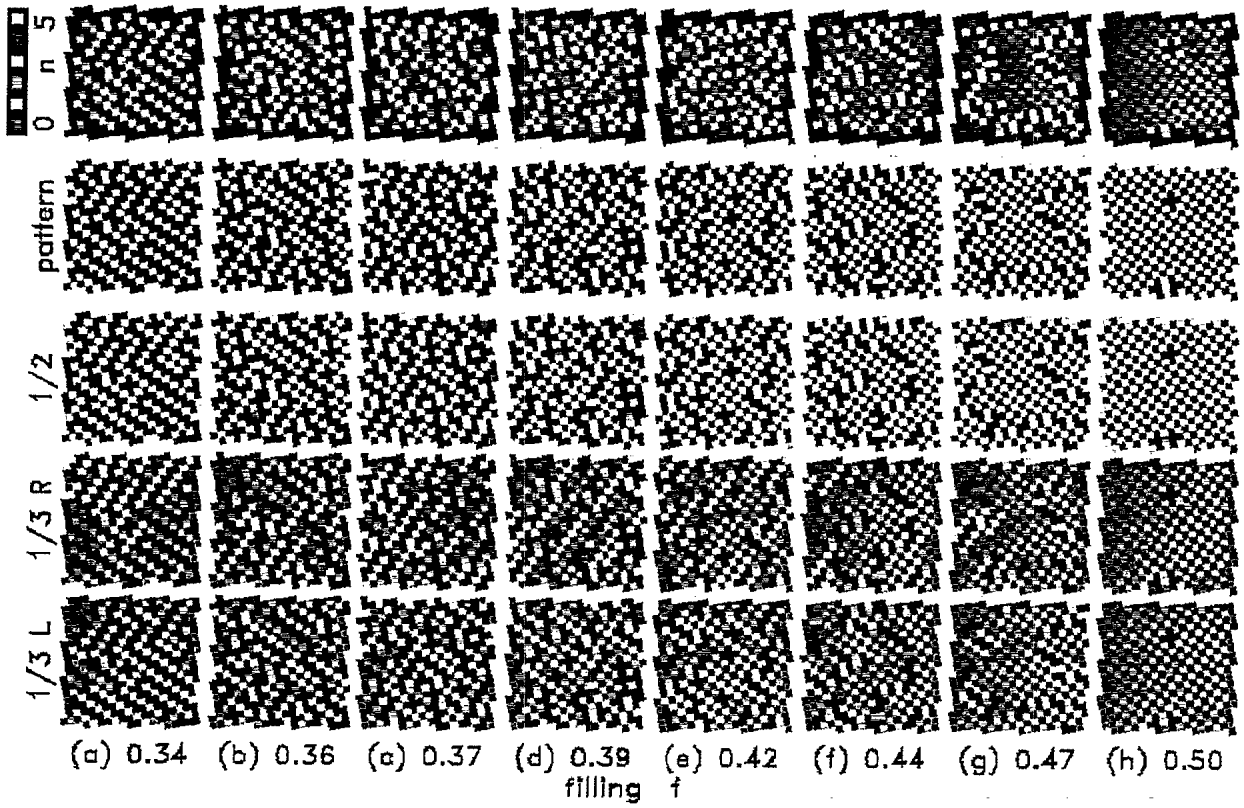

FIG. 2. Evolution of the vortex configuration as filling f varies from 1/3 to 1/2. The row labeled pattern shows the occupation maps at the values of f indicated. In the top row each vortex is assigned a color corresponding to the occupation n of the 8 adjacent sites. The colors used are shown to the left of this row. The row labeled 1/2 highlights domains of the theoretical 1/2 checkerboard ground state which has two phases colored yellow and blue, and the rows labeled 1/3R and 1/3L highlight domains of the two theoretical 1/3 staircase ground states, each of which has three phases colored yellow, blue, and pink (see text).

vortices at arbitrary f in two ways: by coordination and by two-particle positional correlations. These experimental quantities can be compared to the local order of the various theoretical ground states. Deviations between experiment and theory provide a measure of the defects that exist in vortex patterns.

The average vortex coordination evolution of the experiment from $n=2$ near $f=0.33$ to $n=4$ near $f=0.50$ is shown in the top row images of Fig. 2 as a green-yellow-red progression. The probability distributions $P(n)$ of

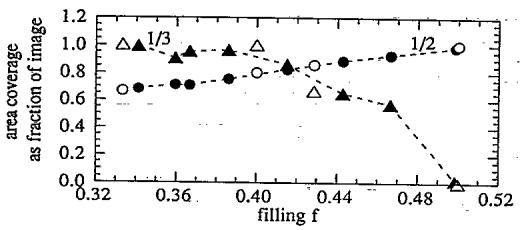

FIG. 3. Fraction of image fit by domains of the theoretical 1/2 checkerboard (black circles) and 1/3 staircase (black triangles) ground states plotted vs f. Open symbols represent the corresponding coverage of single domain 1/2 checkerboard and 3/7, 2/5, and 1/3 staircase ground states predicted in theory.

these images are plotted vs filling in Fig. 4 using the same labels (a) to (h). This can be compared to the probability distribution $P(n)$ of the *theoretical* ground states of the filling sequence 1/3, 2/5, and 1/2 (also shown in Fig. 4, open circles), which are delta functions and unity at $n=2$, 3, and 4. The measured distributions match this progression well, although they appear broadened. The broadening is most pronounced in the higher order fractions: it is maximal at 2/5, followed by 1/3, and smallest at 1/2.

More detail on the local order is provided by the two-particle distribution functions $g(r)$ for vortices (occupied sites) and $e(r)$ for vacancies (empty sites), which are plotted vs spacing r in units of grid size a. For reference, Fig. 4 also includes plots of $g(r)$ and $e(r)$ for the theoretical ground states. Comparing the experimental states labeled (a) through (h) with theoretical states of comparable filling, we find very similar peaks in the distribution functions indicating similar local order. For the JT 1/2 checkerboard state, $g(r)$ and $e(r)$ are identical because the checkerboard pattern is symmetric in the positions of vortices and vacancies. The measured $g(r)$ and $e(r)$ in Fig. 4(h) at $f=0.5$ match theory well. Additional peaks highlight defects in the experimental patterns. For exam-

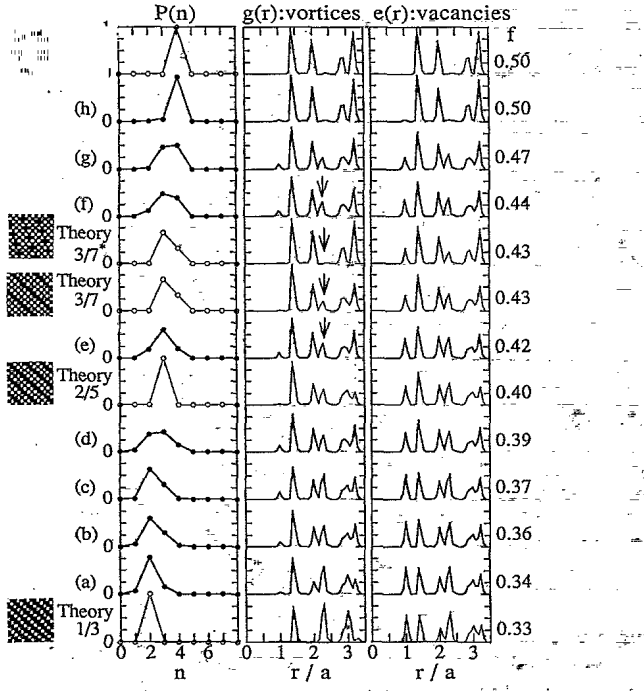

FIG. 4. Probability distributions $P(n)$ of a vortex having coordination n plotted vs n, and two-particle distribution functions $g(r)$ and $e(r)$ for the vortices (occupied sites) and vacancies (empty sites) in the grid, respectively, plotted vs spacing r in units of the grid size a, at the fillings f indicated. The measured traces (a) to (h) correspond to those in Fig. 2. Also shown are traces for the single domain theoretical ground states illustrated at the left; we show the 1/3, 2/5, and 3/7 staircase, the 3/7 vacancy array (labeled 3/7*), and the 1/2 checkerboard ground states (see text).

ple, checkerboard grain boundaries along the grid produce additional peaks in both $g(r)$ and $e(r)$ at $r/a=1$ and $\sqrt{5}$, while vacancies produce these peaks only in $e(r)$ and interstitials produce these peaks only in $g(r)$. As the filling f decreases from 1/2 [Figs. 4(f) and 4(g)] these peaks appear in both $g(r)$ and $e(r)$ and are more prominent in $e(r)$ consistent with the presence of checkerboard grain boundaries and vacancies in the images. We observe a strong peak in $g(r)$ at $r/a=\sqrt{5}$ (see arrows) which is present in the JT 3/7 state but not in the KS 3/7 state, indicating that vortices tend to accumulate at checkerboard grain boundaries rather than within grains. The patterns we observe near $f=3/7$ and $f=2/5$ continue to look like a disordered checkerboard state with grain boundaries and vacancies. We do not observe the predicted 3/7 and 2/5 ground states at these fillings. Close to $f=1/3$ [Fig. 4(a)] the measured $g(r)$ matches that for the JT 1/3 staircase state with additional peaks at 1, 2, and $\sqrt{10}$ due to domain walls between the six degenerate patterns.

Different polycrystalline realizations of a particular vortex ground state at a filling f are thermally frozen in at $T=5$ K. We visualize the vortex motion between different realizations by imaging at 5 K, warming to close to

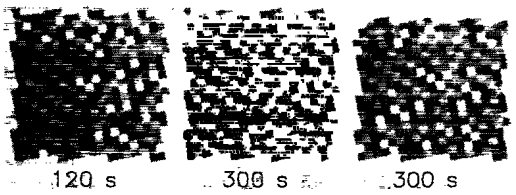

FIG. 5. Vortex occupancy maps near $f=1/3$. Highlighted brighter vortices have moved from highlighted darker vacancies after successive warming to $0.99T_c$.

T_c for 2–5 min, and then recooling for the next image. A sequence of three such warming cycles at $f=0.33$ resulted in the images of Fig. 5. Vortices which moved in each warming cycle are highlighted. Groups of vortices moved together by one unit cell in the same direction. This correlated hopping suggests that fluctuating field gradients with a large spatial length scale are the driving forces. The observed variety in similar low-temperature polycrystalline realizations suggests that a freezing transition close to T_c rather than imperfections in the grid lithography is responsible for the disorder. The lowest temperature where vortex motion is observed (8.7 K) agrees with that derived from an energy barrier argument. As one approaches T_c from below, at 0.1 K below T_c the film penetration depth becomes $\sim$10 times larger than that at 5 K, reducing the energy barrier for an individual vortex hop by $\sim$2–3 orders of magnitude to $\sim 10k_BT_c$ [7,8]. A high freezing temperature may prevent the higher order ground states, such as 2/5, from developing.

*Present address: Department of Physics, North Carolina State University, Raleigh, NC 27695-8202.

[1] Thomas C. Halsey, Phys. Rev. B **31**, 5728 (1985); S. Teitel, Physica (Amsterdam) **152B**, 30 (1988); J. Villain, J. Phys. C **10**, 1717 (1977).

[2] S. Teitel and C. Jayaprakash, Phys. Rev. B **27**, 598 (1983); Phys. Rev. Lett. **51**, 1999 (1983).

[3] Mohammad R. Kolahchi and Joseph P. Straley, Phys. Rev. B **43**, 7651 (1991).

[4] B. Pannetier *et al.*, Phys. Rev. Lett. **53**, 1845 (1984); C. J. Lobb, Physica (Amsterdam) **152B**, 1 (1988), and the other papers therein; M. A. Itzler *et al.*, Phys. Rev. B **42**, 8319 (1990), and the first four references therein.

[5] M. S. Rzchowski, S. P. Benz, M. Tinkham, and C. J. Lobb, Phys. Rev. B **42**, 2041 (1990).

[6] A. M. Chang *et al.*, Appl. Phys. Lett. **61**, 1974 (1992); A. M. Chang *et al.*, Europhys. Lett. **20**, 645 (1992); H. D. Hallen *et al.*, Proc. SPIE Int. Soc. Opt. Eng. (to be published).

[7] The resistivity of $\sim$15 $\mu\Omega$ cm at 10 K implies a short mean free path $\sim$60 Å and a bulk $\lambda\sim$1000 Å. For a thin film 1000 Å geometry the lateral penetration depth is further enhanced by another factor of 2 to give a $\lambda_{\text{eff}}\sim$2000 Å. The penetration depth of a grid patterned film is even longer and such finite sized vortices are described in J. R. Phillips *et al.*, Phys. Rev. B **47**, 5219 (1993).

[8] C. J. Lobb, D. W. Abraham, and M. Tinkham, Phys. Rev. B **27**, 150 (1983).